EUROGRAPHICS 2019 / P. Alliez and F. Pellacini
(Guest Editors)

Volume 38 (2019), Number 2

A Geometrically Consistent Viscous Fluid Solver with Two-Way Fluid-Solid Coupling

Tetsuya Takahashi[†] and Ming C. Lin[*,†]

[†]University of North Carolina at Chapel Hill
[*]University of Maryland at College Park

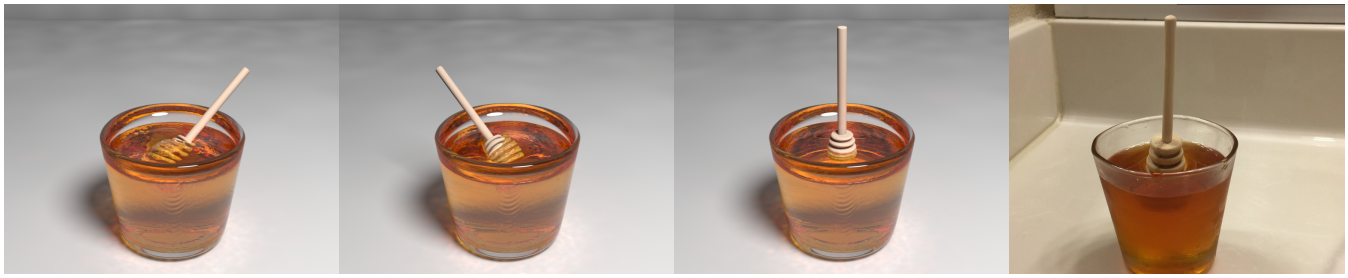

Figure 1: *A wooden honey dipper in the honey. (Left to right): simulated honey with one-way coupling, weak two-way coupling, strong two-way coupling, and the real honey. While the simulated honey using one-way and weak two-way coupling cannot sufficiently support the honey dipper, the simulated honey using our strong two-way coupling can keep the honey dipper standing, as observed in the real phenomena.*

Abstract

We present a grid-based fluid solver for simulating viscous materials and their interactions with solid objects. Our method formulates the implicit viscosity integration as a minimization problem with consistently estimated volume fractions to account for the sub-grid details of free surfaces and solid boundaries. To handle the interplay between fluids and solid objects with viscosity forces, we also formulate the two-way fluid-solid coupling as a unified minimization problem based on the variational principle, which naturally enforces the boundary conditions. Our formulation leads to a symmetric positive definite linear system with a sparse matrix regardless of the monolithically coupled solid objects. Additionally, we present a position-correction method using density constraints to enforce the uniform distributions of fluid particles and thus prevent the loss of fluid volumes. We demonstrate the effectiveness of our method in a wide range of viscous fluid scenarios.

CCS Concepts

• ***Computing methodologies*** → *Physical simulation;*

1. Introduction

Viscous fluids, such as honey, molten chocolate, paint, oil, and shampoo, are common materials as frequently seen in daily life. These viscous materials exhibit characteristic behaviors including damped and sticky motions and buckling phenomena, both of which are not observed for inviscid fluids. Because of the ubiquity of viscous fluids and their fascinating behaviors, simulating viscous fluids has been needed in a variety of applications e.g., video games, feature films, and virtual reality. Various researchers have proposed simulation methods specifically designed for viscous fluids [CMVHT02, REN*04, BB08, BAV*10, BUAG12, ZLQF15, TDF*15, PICT15, LBB17].

In the previous works, several compelling viscous fluid behaviors have been demonstrated focusing primarily on simulating the intriguing behaviors of viscous fluids induced by the gravitational forces with static or prescribed solid boundaries. However, mutual interactions between viscous fluids and solid objects are essential, and thus it is necessary to correctly handle such interactions. In the literature, there are various approaches presented to simulate the interactions of *inviscid* fluids and solids objects [CMT04, KFCO06, CGFO06, BBB07, RMSG*08, LJF16, TLK16, ZB17]. These approaches enable the two-way interactions between fluids and solid objects with pressure forces, which play roles of drag and buoyancy forces. The pressure forces can be sufficient to describe the interactions between nearly inviscid fluids and solid objects. However, simulating the interactions between highly viscous fluids and solid objects with only pressure forces leads to fluid and solid behaviors significantly different from those observed in the real world, and it is necessary to consider *viscosity* forces to correctly account for the two-way interactions.

In this paper, we present a grid-based fluid solver that can handle two-way interactions of fluids and solid objects with viscosity forces. Our method formulates the dynamics of viscous fluids and solid objects as a unified minimization problem based on the

© 2019 The Author(s)
Computer Graphics Forum © 2019 The Eurographics Association and John Wiley & Sons Ltd. Published by John Wiley & Sons Ltd.

variational principle, and thus achieves the correct behaviors for both fluids and solids. To improve the accuracy even on relatively coarse grids, we estimate volume fractions of free surfaces and solid boundaries in a geometrically consistent way and formulate our method with these fractions accounting for the sub-grid level details. In our method, we use Lagrangian particles to discretize the fluid volumes and address the advection by moving particles. While the combination of particles and a grid is proven to be effective [Bri15], one known issue is that the distributions of particles would be non-uniform leading to the loss of fluid volumes and producing gaps and holes in the fluids. In addition, the interactions with solids can make the particle distributions even more non-uniform further causing undesirable volume changes. To address this issue, we propose a position-correction method based on density constraints at the particle level to enforce the uniform particle distributions. In summary, our method offers the following key contributions:

- **A geometrically consistent volume fraction estimation** that utilizes the supersampling technique to improve the accuracy of the simulation and avoids dangling artifacts near free surfaces and solid boundaries (§ 3.3).
- **A two-way fluid-solid coupling using viscosity force** that robustly and correctly accounts for the dynamics of viscous fluids and solid objects through their interactions (§ 3.4).
- **A position-correction method** using density constraints with a position-correction scaling that enforces the uniform particle distributions avoiding non-physical volume changes (§ 3.5).

We integrate these techniques with a viscous fluid solver. Figure 1 demonstrates complex interactions of viscous fluids and solid objects simulated with our method.

2. Related Work

In this section, we discuss previous works closely related to ours. We refer to [Bri15] for the literature and fundamentals.

2.1. Viscous Fluids

In the Eulerian framework, an early work, stable fluid method [Sta99] solved the Navier-Stokes equations with implicit viscosity integration for numerical stability while focusing on fluids without free surfaces. Carlson et al. [CMVHT02] proposed the first method for simulating highly viscous fluids with free surfaces by using a simplified, Laplacian-based viscosity model with implicit integration. However, the Laplacian-based formulation immediately damps the rotational velocity fields due to incorrect free surface boundary conditions. Later, Rasmussen et al. [REN*04] augmented the Laplacian-based formulation by adding off-diagonal components with explicit integration while sacrificing the robustness. Batty and Bridson [BB08] proposed a fully implicit integration scheme for the full form of viscosity with correct free surface boundary conditions and made it possible to simultaneously take larger time steps, handle variable viscosity, and generate rotational fluid motions. Later, this method was extended for an adaptive tetrahedral fluid simulator [BH11]. Recently, Larionov et al. [LBB17] proposed a pressure-viscosity coupled solver to further improve the accuracy in the free surface handling. While Robinson-Mosher et al. [RMSF11] also presented a pressure-viscosity coupled solver, their approach focused on fluids without free surfaces adopting the Laplacian-based viscosity formulation with the voxel-based discretization. Although the previous methods [BB08, LBB17] used volume fractions for the sub-grid level accuracy, they did not address how to consistently estimate control volumes of fluids and solids for velocity and viscous stress.

To simulate more general fluids, e.g., viscoelastic fluids and non-Newtonian fluids, various approaches were also proposed. Goktekin et al. [GBO04] presented a method for simulating viscoelastic fluids by adding an extra term for elastic forces. Recently, to handle fluid-like materials with a variety of properties in a unified way, material point methods (MPM) have been widely adopted with some specialized extensions for snow [SSC*13], foams [YSB*15], melting solids [SSJ*14], and granular materials [DBD16, KGP*16, JGT17, TGK*17, GPH*18, HFG*18]. While these approaches allow us to simulate a wide range of materials, the constitutive laws adopted in these works typically involve the non-linearity which would cause stability issues with explicit integration or requires expensive non-linear solves for implicit integration. Thus, in this paper, we focus on purely Newtonian viscous fluids, whose dynamics on viscosity can be simulated with only linear solves.

In the Lagrangian framework, various approaches have been also proposed to simulate viscous fluids. Specifically, particle-based methods based on Smoothed Particle Hydrodynamics (SPH) have been widely used, and recently, various extensions were presented to improve the robustness and efficiency of the viscosity integration [TDF*15, PICT15, BK16, PT17, BGFAO17, WKBB18]. In the Lagrangian setting, some researchers proposed dimension-reduced representations to capture the detailed dynamics of viscous threads and sheets [BAV*10, BUAG12, ZLQF15]. While our method employs Lagrangian particles for advection, surface tracking, and volume preservation, the dynamics is computed on a grid unlike these purely Lagrangian approaches.

2.2. Two-Way Fluid-Solid Coupling

For coupling of Eulerian fluids with Lagrangian solids, early works, e.g., [GSLF05] achieved the two-way coupling with pressure forces by alternatively solving one-way fluid-to-solid and solid-to-fluid coupling, which is known as weak two-way coupling. While the weak coupling would work in certain scenarios, the stability of the simulation is not guaranteed, and it is generally necessary to take very small time steps with many alternate one-way solves. Carson et al. [CMT04] presented a two-way coupling method that temporarily treats solid objects as fluids in the pressure solve sacrificing the robustness. Chentanez et al. [CGFO06] presented a two-way coupling method that simultaneously considers both dynamics of fluids and deformable solids, which is known as strong two-way coupling. While their method improves the stability, the resulting linear system is not symmetric. Klingner et al. [KFCO06] also proposed a two-way coupling approach with dynamic meshes. While their linear system is symmetric positive definite (SPD), the computational cost is likely to be expensive due to the dynamic meshes. Batty et al. [BBB07] presented a strong two-way coupling method with the Cartesian grid based on the variational principle and significantly improved the efficiency. Later, this method was extended for frictional forces [NGL10]. Robinson-Mosher et al. [RMSG*08]

© 2019 The Author(s)
Computer Graphics Forum © 2019 The Eurographics Association and John Wiley & Sons Ltd.

also presented a two-way coupling approach with a more accurate momentum handling than [BBB07]. Later, they extended their approach to improve the accuracy of tangential velocities [RMEF09] and to generate an SPD system with the Laplacian form of viscosity [RMSF11], and the performance of this approach was improved with a multigrid preconditioning [Aan18]. Recently, strong two-way coupling was employed for interactions between deformable solids and fluids [LJF16, TLK16, ZB17], interactions between rigid bodies and fluids simulated using a vorticity-based fluid solver [VHLL14] and a stream function solver [ATW15], while weak two-way coupling was augmented with the reduced model interface to improve the stability [ANZS18].

In the MPM framework, collisions between fluids and other objects can be naturally handled at the grid level. Because of this advantage, MPM is widely adopted to simulate two-way interactions with rigid bodies [DBD16, HFG*18] and with deformable solids [KGP*16, JGT17]. Since solid objects are typically described in a Lagrangian setting, Lagrangian particle-based methods are also extensively used, and the two-way coupling can be achieved in a unified way [SSP07, AIA*12, MMCK14].

While there are various two-way coupling methods proposed for Eulerian fluids and Lagrangian solids, most of these approaches focus on two-way coupling with pressure forces, but not viscosity forces. Although Robinson-Mosher et al. [RMSF11] presented a two-way coupling method with viscosity force, their formulation relies on the Laplacian form of viscosity (which precludes rotational behaviors of viscous fluids) and focuses on voxel-based discretization with no free surfaces. In contrast to these approaches, our method focuses on two-way coupling with *viscosity* forces formulated using the *full* form of viscosity with free surfaces taking volume fractions into account for sub-grid details.

3. Our Method

In this section, we describe our fluid solver using the implicit viscosity integration. We formulate the viscosity integration as a minimization problem based on the variational principle (§ 3.1) so that the minimization problem can be naturally discretized with volume fractions to account for the sub-grid level details (§ 3.2). To avoid dangling artifacts, we describe our geometrically consistent volume estimation (§3.3). Next, we present a two-way coupling formulation, which can be efficiently solved with the minimization problem in a unified way (§ 3.4). Then, we describe a position-correction method using density constraints to enforce the uniform distributions of particles (§ 3.5). Finally, we discuss previously proposed methods vs. ours to clarify key differences (§ 3.6).

3.1. Implicit Viscosity Formulation

The incompressible Navier-Stokes equations are given by

$$\frac{D\mathbf{u}}{Dt} = -\frac{1}{\rho}\nabla p + \frac{1}{\rho}\nabla\cdot\mathbf{s} + \frac{1}{\rho}\mathbf{f}, \quad \mathbf{s} = \eta\left(\nabla\mathbf{u} + (\nabla\mathbf{u})^T\right), \quad \nabla\cdot\mathbf{u} = 0,$$

where t denotes time, $\frac{D}{Dt}$ material derivative, $\mathbf{u}$ velocity, ρ density, p pressure, $\mathbf{s}$ symmetric viscous stress tensor, $\mathbf{f}$ external force, and η dynamic viscosity. We address the advection term with the affine particle-in-cell (APIC) approach [JSS*15] and take the operator splitting method to handle external force, pressure, and viscosity terms, applying solid boundary condition $\mathbf{u}^{t+1} = \mathbf{u}^{\text{solid}}$ ($\mathbf{u}^{\text{solid}}$: solid boundary velocity) and free surface boundary condition $\mathbf{sn} = 0$ ($\mathbf{n}$: outward unit normal of the free surface) for the viscosity solve [BB08].

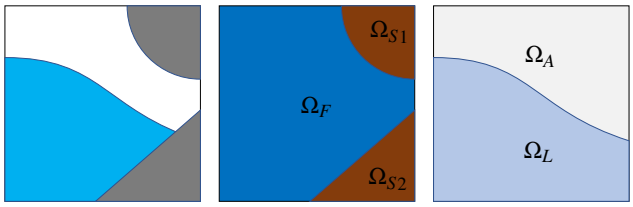

Figure 2: *Domain illustration. (Left) The simulation domain Ω is filled with viscous fluids (cyan), solid objects (gray), and the rest (white). (Middle) The simulation domain is separated by the solid boundaries into multiple solid (brown) and fluid (blue) domains. (Right) The simulation domain is separated by the free surfaces into liquid (light blue) and air (light gray) domains.*

The viscosity update with backward Euler can be written as

$$\frac{\mathbf{u}^{t+1}-\mathbf{u}^*}{\Delta t} = \frac{1}{\rho}\nabla\cdot\mathbf{s}^{t+1}, \quad \mathbf{s}^{t+1} = \eta\left(\nabla\mathbf{u}^{t+1} + \left(\nabla\mathbf{u}^{t+1}\right)^T\right),$$

where $\mathbf{u}^*$ denotes intermediate velocity after advection, external force, and first pressure projection steps [BB08], and Δt time step size. In the following, we omit superscript $t+1$ for readability. These formulations can be cast as a minimization problem due to the variational principle [BBB07, BB08, LBB17]:

$$\mathbf{s} = \arg\min_{\mathbf{s}} \int_{\Omega_F} \left(\frac{\rho}{2}\|\mathbf{u}^* + \frac{\Delta t}{\rho}\nabla\cdot\mathbf{s}\|^2 + \frac{\Delta t}{4\eta}\|\mathbf{s}\|_F^2\right) d\Omega, \quad (1)$$

where Ω_F denotes the fluid domain (see Figure 2), $\|\cdot\|_F$ the Frobenius norm. When dynamic viscosity η approaches to 0, viscous stress $\mathbf{s}$ (which includes η) also approaches to $\mathbf{0}$, and this minimization preserves intermediate velocity $\mathbf{u}^*$ (i.e., no viscosity force applied). On the other hand, when η approaches to ∞, optimal viscous stress are sought by minimizing the sum of these two terms. This will eventually prioritize the first term due to $\mathbf{s}$'s quadratic property with respect to η and make the term 0, giving certain viscous stress which leads to $\mathbf{u}$ $(= \mathbf{u}^* + \frac{\Delta t}{\rho}\nabla\cdot\mathbf{s}) = \mathbf{0}$.

3.2. Discretization

To discretize Eq. (1), we approximate the integral in the minimization with fractions of cell-sized control volumes. Given solid boundaries defined with signed distance functions (SDF), simulation domain Ω is divided into multiple solid domains $\Omega_{S1}, \Omega_{S2}, \ldots, \Omega_{Sn}$ (n: number of solid objects) and fluid domains Ω_F, (i.e., $\cup_i^n \Omega_{Si} \cup \Omega_F = \Omega$, $\Omega_{Si} \cap \Omega_{Sj} = \phi$, and $\Omega_{Si} \cap \Omega_F = \phi$, where i, j $(i \neq j)$ denote an index for solid domains), as illustrated in Figure 2. Following the notations in [LBB17], we denote volume fractions for solid and fluid domains as diagonal matrices $\mathbf{W}_S^u$ and $\mathbf{W}_F^u$, respectively. We note that $\mathbf{W}_S^u$ is defined for each solid object, i.e., $\mathbf{W}_{S1}^u, \ldots, \mathbf{W}_{Sn}^u$ and $\sum_i \mathbf{W}_{Si}^u + \mathbf{W}_F^u = \mathbf{I}$. As for viscous stress defined in a staggered manner [GBO04], we also compute volume fractions for solid domains $\mathbf{W}_S^s$ and fluid domains $\mathbf{W}_F^s$.

Similar to [LBB17], we can formulate a minimization problem

© 2019 The Author(s)
Computer Graphics Forum © 2019 The Eurographics Association and John Wiley & Sons Ltd.

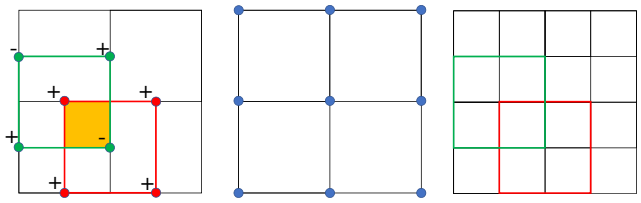

Figure 3: *(Left) Illustration for inconsistent volumes with the independent volume estimation. Red and green squares represent u- and v-cells, respectively, and orange filled square represents an overlapping region between u- and v-cells. Red and green dots represent cell nodes, where SDF are evaluated for the volume computation of u- and v- cells, respectively. + and - represent signs of SDF at the node positions. (Middle) Simulation grid, where SDF for both solid boundaries and free surfaces are defined on the grid nodes (blue dots). (Right) Double-resolution grid, where volumes of each cell consistently contribute to the volume summation of u- (red) and v- (green) cells on the simulation grid.*

for liquid domains (Figure 2), corresponding to Eq. (1). For discretization, as done for solid/fluid volume fractions, we can consider air/liquid volume fractions. Since free surfaces separate the simulation domain Ω into liquid domains Ω_L and air domains Ω_A, we also compute volume fractions for velocity components of liquid domains $\mathbf{W}_L^u$ and air domains $\mathbf{W}_A^u$ ($\mathbf{W}_L^u + \mathbf{W}_A^u = \mathbf{I}$), and viscous stress components of liquid and air domains as $\mathbf{W}_L^s$ and $\mathbf{W}_A^s$, respectively.

Combining the minimization formulations for fluid domains and liquid domains [LBB17], we obtain the following discretized minimization problem:

$$\mathbf{s} = \arg\min_{\mathbf{s}} \Big(\frac{1}{2} \| (\mathbf{P}\mathbf{W}_F^u \mathbf{W}_L^u)^{\frac{1}{2}} (\mathbf{u}^* - \Delta t \mathbf{P}^{-1} \mathbf{W}_L^{u-1} \mathbf{D}^T \mathbf{W}_L^s \mathbf{s}) \|^2 + \frac{\Delta t}{4} \mathbf{N}^{-1} \| (\mathbf{W}_F^s \mathbf{W}_L^s)^{\frac{1}{2}} \mathbf{s} \|^2 \Big), \quad (2)$$

where $\mathbf{P}$ denotes a diagonal density matrix, $\mathbf{D}$ a discrete finite-difference operator, $\mathbf{N}$ a diagonal dynamic viscosity matrix.

3.3. Geometrically Consistent Volume Estimation

While we can compute volume fractions $\mathbf{W}_F^u, \mathbf{W}_L^u, \mathbf{W}_F^s$, and $\mathbf{W}_L^s$ for each cell *independently*, we found that evaluating these volume fractions in this way causes some artifacts near solid boundaries and free surfaces (e.g., dangling fluid particles in the air) due to the inconsistency of the estimated volumes over the domain. For example, as illustrated in Figure 3 (left), since volumes for u-cell (red) and v-cell (green) are independently evaluated with SDF at their cell nodes (red and green dots for u- and v-cells, respectively), it would happen that the u-cell has zero volumes (all signs of SDF are plus) while the v-cell has non-zero volumes leading to the volume inconsistency at the overlapping region (orange filled square).

To avoid this issue, we evaluate volume fractions in a geometrically consistent manner. We first construct a grid with a doubled resolution compared to the simulation grid, and evaluate volume fractions of the cells on the double-resolution grid with SDF defined on each node of the simulation grid (see Figure 3). Next, we sum up these volume fractions computed on the double-resolution grid to account for one volume fraction for the simulation grid, i.e., in 2D, we sum up four volume fractions on the double-resolution grid to account for *u*- and *v*- cells emphasized by red and green squares, respectively, in Figure 3 (right). Since volume fractions of each cell on the double-resolution grid consistently contribute to the volume summation on the simulation grid, this approach enforces the volume consistency over the domain.

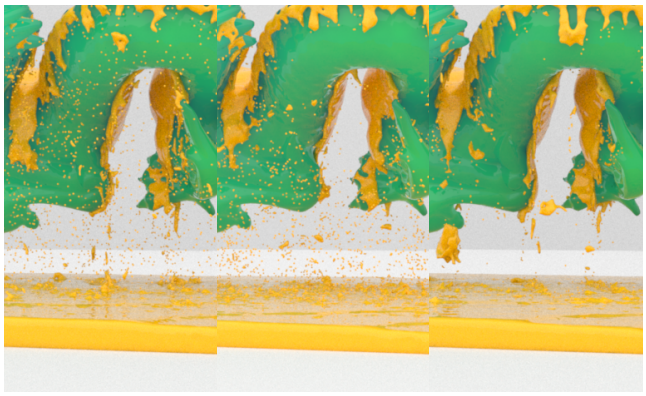

Figure 4: *A viscous ball dropped onto a static, tilted solid dragon. The independent volume estimation causes artifacts that particles unnaturally float under the dragon due to the inconsistent volumes (left), and the supersampling method similarly suffers from the artifacts due to the inaccurate volume estimation (middle), whereas our geometrically consistent volume estimation method does not have such issues (right).*

The volume fractions for viscous stress can be similarly estimated by summing up the fractions computed on the double-resolution grid, and these computations can be naturally extended into 3D. In 2D, we evaluate the volume fractions using a marching-squares-style area computation method. In 3D, we use a volume computation algorithm using the divergence theorem [Wan13], which was around five times faster than the volume computation based on the tetrahedral decomposition [MG07].

Our volume estimation approach can be considered as a generalized version of the volume estimation using the supersampling method that determines the fluid volumes based on level-set values at specific points [Bri15], and we found that a similar consistent volume computation method was recently used in [Bat08] employing the volume computation based on [MG07], unlike our method based on [Wan13].

3.4. Strong Two-Way Fluid-Solid Coupling

Similar to [NGL10], we can describe a rigid body update due to the viscous stress applied from fluids with volume fractions by

$$\mathbf{V}^{t+1} = \mathbf{V}^t + \Delta t \mathbf{M}^{-1} \mathbf{W}_S^u \mathbf{J} \mathbf{W}_L^s \mathbf{s}, \quad (3)$$

where $\mathbf{V} \in \mathbb{R}^6$ denotes a generalized rigid body velocity, $\mathbf{M}$ a diagonal, generalized rigid body mass matrix, and $\mathbf{J}$ a linear operator which integrates viscous stresses over the surface of the rigid body to give viscosity forces. The rigid body update can be also cast as a

© 2019 The Author(s)
Computer Graphics Forum © 2019 The Eurographics Association and John Wiley & Sons Ltd.

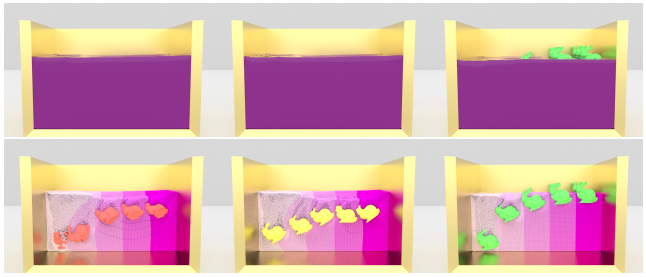

Figure 5: *Multiple solid bunnies dropped onto fluids with spatially different viscosity values* $\eta = 1.0\times10^1, 1.0\times10^2, 1.0\times10^3, 1.0\times10^4$, *and* 1.0×10^8 kg/(s·m). *From left to right, one-way coupling, weak two-way coupling, and our strong two-way coupling, for rendered fluid surfaces (Top) and particle view, color-coded based on viscosity values (Bottom), where white and purple represent low and high viscosity values, respectively. Fluids simulated with one-way coupling and weak two-way coupling do not sufficiently reflect different viscosity values, whereas fluid simulated with strong two-way coupling correctly does.*

minimization problem [BBB07, NGL10], and due to the minimization problem for fluids (Eq. (2)), we can naturally integrate these problems into the following, which monolithically couples viscous fluid and rigid body dynamics:

$$\mathbf{s} = \arg\min_{\mathbf{s}} \Big(\frac{1}{2} \|(\mathbf{P}\mathbf{W}_F^u \mathbf{W}_L^u)^{\frac{1}{2}} (\mathbf{u}^* - \Delta t \mathbf{P}^{-1} \mathbf{W}_L^{u\,-1} \mathbf{D}^T \mathbf{W}_L^s \mathbf{s})\|^2 + \frac{\Delta t}{4} \mathbf{N}^{-1} \|(\mathbf{W}_F^s \mathbf{W}_L^s)^{\frac{1}{2}} \mathbf{s}\|^2 + \frac{1}{2} \|\mathbf{M}^{\frac{1}{2}} (\mathbf{V}^t + \Delta t \mathbf{M}^{-1} \mathbf{W}_S^u \mathbf{J} \mathbf{W}_L^s \mathbf{s})\|^2 \Big).$$

This minimization problem is quadratic, and its optimality condition leads to the following symmetric positive definite (SPD) linear system for $\mathbf{s}$:

$$\Big(\frac{1}{2} \mathbf{N}^{-1} \mathbf{W}_F^s \mathbf{W}_L^s + \Delta t \mathbf{W}_L^s \mathbf{D} \mathbf{P}^{-1} \mathbf{W}_L^{u\,-1} \mathbf{W}_F^u \mathbf{D}^T \mathbf{W}_L^s + \Delta t \mathbf{W}_L^s \mathbf{J}^T \mathbf{W}_S^u \mathbf{M}^{-1} \mathbf{W}_S^u \mathbf{J} \mathbf{W}_L^s \Big) \mathbf{s} = \mathbf{W}_L^s \mathbf{D} \mathbf{W}_F^u \mathbf{u}^* - \mathbf{W}_L^s \mathbf{J} \mathbf{W}_S^u \mathbf{V}^t. \quad (4)$$

Although this system is SPD, the size of the system is very large (approximately $6H \times 6H$ ignoring the relatively small number of DOFs for rigid bodies, where H denotes number of total simulation voxels), and partly dense due to the two-way coupled solid objects [BBB07, RMSG*08, Bri15]. Given $\mathbf{u} = \mathbf{u}^* - \Delta t \mathbf{P}^{-1} \mathbf{W}_L^{u\,-1} \mathbf{D}^T \mathbf{W}_L^s \mathbf{s}$ and Eq. (3), we can reformulate the system above with unknown variables $\mathbf{u}$, $\mathbf{s}$, and $\mathbf{V}$ as

$$\begin{pmatrix} \frac{\mathbf{P}}{\Delta t} \mathbf{W}_F^u \mathbf{W}_L^u & \mathbf{W}_F^u \mathbf{D}^T \mathbf{W}_L^s & 0 \\ \mathbf{W}_L^s \mathbf{D} \mathbf{W}_F^u & -\frac{1}{2} \mathbf{N}^{-1} \mathbf{W}_F^s \mathbf{W}_L^s & -\mathbf{W}_L^s \mathbf{J}^T \mathbf{W}_S^u \\ 0 & -\mathbf{W}_S^u \mathbf{J} \mathbf{W}_L^s & \frac{\mathbf{M}}{\Delta t} \end{pmatrix} \begin{pmatrix} \mathbf{u} \\ \mathbf{s} \\ \mathbf{V} \end{pmatrix} = \begin{pmatrix} \frac{\mathbf{P}}{\Delta t} \mathbf{W}_F^u \mathbf{W}_L^u \mathbf{u}^* \\ 0 \\ \frac{\mathbf{M}}{\Delta t} \mathbf{V}^t \end{pmatrix}.$$

From this system, we can reduce the system size by taking the Schur complement of the diagonal block matrix for the viscous stress (eliminating $\mathbf{s}$ from the system), and we obtain the following linear system for $\mathbf{u}$ and $\mathbf{V}$:

$$\begin{pmatrix} \mathbf{A}_{11} & \mathbf{A}_{12} \\ \mathbf{A}_{12}^T & \mathbf{A}_{22} \end{pmatrix} \begin{pmatrix} \mathbf{u} \\ \mathbf{V} \end{pmatrix} = \begin{pmatrix} \frac{1}{\Delta t} \mathbf{P} \mathbf{W}_F^u \mathbf{W}_L^u \mathbf{u}^* \\ \frac{\mathbf{M}}{\Delta t} \mathbf{V}^t \end{pmatrix},$$

$$\mathbf{A}_{11} = \frac{1}{\Delta t} \mathbf{P} \mathbf{W}_F^u \mathbf{W}_L^u + 2 \mathbf{W}_F^u \mathbf{D}^T \mathbf{W}_L^s \mathbf{N} \mathbf{W}_F^{s\,-1} \mathbf{D} \mathbf{W}_F^u.$$

$$\mathbf{A}_{12} = -2 \mathbf{W}_F^u \mathbf{D}^T \mathbf{W}_L^s \mathbf{N} \mathbf{W}_F^{s\,-1} \mathbf{J}^T \mathbf{W}_S^u.$$

$$\mathbf{A}_{22} = \frac{\mathbf{M}}{\Delta t} + 2 \mathbf{W}_S^u \mathbf{J} \mathbf{N} \mathbf{W}_F^{s\,-1} \mathbf{W}_L^s \mathbf{J}^T \mathbf{W}_S^u.$$

This linear system can be more efficiently solved than Eq. (4) because the resulting system is still SPD, the system size is much smaller (approximately $3H \times 3H$), the system matrix is sparser due to $\mathbf{V}$ treated as unknown variables even though fluid and solid dynamics are monolithically coupled [RMSG*08, Bri15].

3.5. Position Correction

The divergence-free velocity fields enforce the constant volumes of fluids in the continuous setting. In practice, however, fluid volumes can change due to the spatial and temporal discretization involving numerical errors, as a volume correction method was proposed to address this issue for Eulerian fluid simulation with the level-set surface tracking [KLL*07]. Given Lagrangian particles used for tracking surfaces in our method, to preserve the fluid volumes, it is necessary to enforce the uniform distribution of particles, which also addresses the gap and holes caused by non-uniform particle distributions [Bri15]. While some position-correction methods have been previously proposed [AT11, UBH14], we found that damped motions of viscous fluids make the volume changes noticeable more easily and require more uniform particle distributions. To this end, we present a position-correction method using density constraints motivated by the purely Lagrangian SPH work [MMCK14].

We define the density constraint per particle with particle density ρ_i and the rest density ρ_0 as

$$C_i = \max\left(\frac{\rho_i}{\rho_0} - 1, 0 \right),$$

where ρ_i is computed by $\rho_i = m_i \sum_j w_{ij}(\mathbf{x})$ with particle mass m and position $\mathbf{x}$ and the smoothing kernel w using the traditional summation approach in SPH. Solving the constraints by correcting particle positions can be formulated as a minimization problem:

$$\Delta \mathbf{x} = \arg\min_{\Delta \mathbf{x}} \frac{1}{2} \Delta \mathbf{x}^T \mathbf{A} \Delta \mathbf{x}, \quad \text{subject to } C(\mathbf{x} + \Delta \mathbf{x}) = 0,$$

where $\Delta \mathbf{x}$ denotes the position correction, $\mathbf{A}$ mass matrix for particles, and we can compute the position correction locally following [MMCK14] by

$$\Delta \mathbf{x}_i = -\frac{C_i \mathbf{A}^{-1} \nabla C_i^T}{\nabla C_i \mathbf{A}^{-1} \nabla C_i^T}.$$

Although correcting particle positions with this correction vector would work, many iterations are necessary in most cases. This is because this method tries to satisfy the constraints by pushing particles into the solids although these particles are again projected back to the solid surfaces using the level-set ϕ by $\mathbf{x} := \mathbf{x} - \phi \frac{\nabla \phi}{\|\nabla \phi\|}$ without caring about the particle density at the projected position.

© 2019 The Author(s)
Computer Graphics Forum © 2019 The Eurographics Association and John Wiley & Sons Ltd.

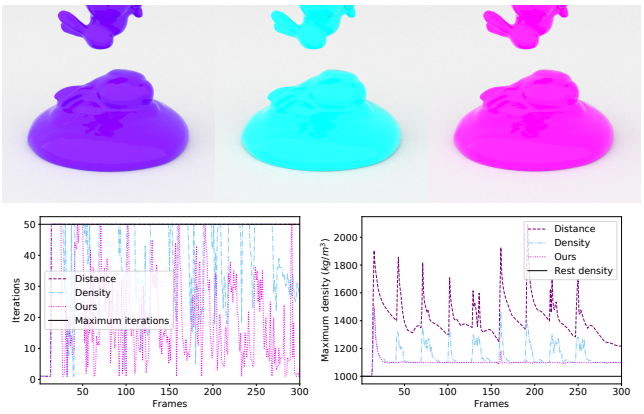

Figure 6: *(Top) Pileup of multiple viscous bunnies simulated using the distance constraint (left), density constraint without (middle) and with (right) the scaling based on the distance to solid boundaries. (Bottom) Profiles of the iteration counts (left) and maximum density (right). The density constraint converges faster, and the scaling accelerates the convergence of the density constraints.*

Considering this fact, to reduce necessary iterations, we allow particles farther from solid boundaries to move more distances. This approach is motivated by the mass-splitting [TBV12] and mass-scaling [MMCK14]. We define the scaling factor α based on the distance to solid boundaries clamping it to avoid instability as

$$\alpha_i = \mathrm{clamp}(\phi(\mathbf{x}_i)/\theta, \alpha_{\min}, \alpha_{\max}),$$

where θ denotes the grid width and $\alpha_{\min}$ and $\alpha_{\max}$ the minimum and maximum values for α, respectively. We typically use $\alpha_{\min} = 1.0$ and $\alpha_{\max} = 5.0$. With the scaling, we correct the particle positions by

$$\mathbf{x}_i^{l+1} = \mathbf{x}_i^l + \alpha_i \Delta \mathbf{x}_i^l,$$

where l denotes an iteration index. The effectiveness of the scaling is demonstrated in Figure 6, which compares our method with the distance and density constraints based on [AT11] and [MMCK14], respectively.

3.6. Discussions

At the continuous formulation level, the resulting system of our method for viscous fluid dynamics is closely related to the work of [BB08], and our method can be considered as an augmented version of their method with geometrically consistent volume fractions for both solid boundaries and free surfaces to more accurately account for sub-grid details. In addition, we proposed the two-way coupling method to achieve interactions between highly viscous fluids and solid objects, and presented the position-correction method to address the non-uniform particle distributions.

While our formulation and its interpretation are inspired by the work of [LBB17], these formulations are different in that our method decouples the pressure and viscosity solves while their method couples these. As reported in [LBB17], these different formulations have advantages and disadvantages. For example, the decoupled approach is more efficient whereas this approach cannot faithfully reproduce coiling phenomena nor preserve surface details, and vice versa. In this work, we chose the decoupled approach mainly for efficiency. However, our position-correction method can be naturally integrated into the coupled solver [LBB17], and the two-way coupling method can be unified as well forming an SPD system with dense blocks for stress variables or a sparse indefinite system for pressure and velocity variables.

4. Results and Discussions

All the examples are executed on a Linux machine with 24-core 2.50GHz Intel Xeon and 256GB RAMs. For the viscosity solve, we use Modified Incomplete Cholesky Conjugate Gradient (MICCG) and set the convergence criterion as the infinity norm of the relative residual 1.0×10^{-10}. We used the CFL number of 3.0 with the adaptive time stepping. We performed the position correction once per frame with the termination criteria (tolerance) as 10% of the rest density. Simulation conditions and performance are summarized in the supplementary material.

4.1. Volume Estimation

We compared our geometrically consistent volume evaluation method with a method that independently estimates volume fractions and the supersampling-based method [Bri15]. We use a scenario, where a viscous ball is dropped onto a static, tilted dragon, as shown in Figure 4. With the independent volume estimation, the estimated volumes can be inconsistent over the domain, and fluid/solid and liquid/air domains can be erroneously evaluated. Consequently, the viscosity solve would generate non-physical velocity fields leading to the artifacts that particles unnaturally float in the air. With the supersampling method, although the volume estimation can be consistent over the domain, the estimated volumes are not accurate enough since this approach relies on volume estimation at specific points only. Consequently, similar to the independent volume estimation, particles can be unnaturally left in the air. In contrast, our method enforces the volume consistency over the domain achieving more accurate estimations and does not suffer from the artifacts with a little additional cost (approximately 13% more costly for the volume computation than the inconsistent version and the supersampling method leading to only about 5% overhead for the total computation time).

4.2. Two-Way Fluid-Solid Coupling

To validate the accuracy of our strong two-way coupling for viscosity, we first experimented with a simple scenario, where a solid ball is falling inside of viscous fluids, so that analytical solutions of the solid velocity can be computed. We use fluid viscosity values $\eta = 1.0 \times 10^1, 1.0 \times 10^2, 1.0 \times 10^3, 1.0 \times 10^4$, and 1.0×10^5 kg/(s·m) with fluid density $\rho_f = 1.0 \times 10^3$ kg/m^3, solid density $\rho_s = 3.0 \times 10^3$ kg/m^3, and the radius of the solid ball $r = 5.0 \times 10^{-2}$ m. We compare our method with one-way coupling from solid-to-fluid, weak two-way coupling (viscosity solve followed by an implicit solid velocity update), and the analytical solution derived from the Stokes' law. As for pressure forces, we achieve strong two-way coupling based on the works of [BBB07,NMG09]. Figure 7 shows the comparison executed with $\eta = 1.0 \times 10^3$ kg/(s·m). For one-way and weak two-way coupling,

© 2019 The Author(s)
Computer Graphics Forum © 2019 The Eurographics Association and John Wiley & Sons Ltd.

Table 1: *Simulation conditions and results for Figure 7. Re: Reynolds number, $\hat{V}^{\infty}$: analytical terminal velocity magnitude of the ball, $V^{\infty}_{\text{oneway}}$, V^{∞}_{weak}, $V^{\infty}_{\text{strong}}$: averaged terminal velocity magnitude at equilibrium from the simulation with one-way, weak two-way, and strong two-way coupling, respectively. $\varepsilon_{\text{oneway}}$, $\varepsilon_{\text{weak}}$, $\varepsilon_{\text{strong}}$: relative errors for one-way, weak two-way, and strong two-way coupling, respectively. The gray row means that Stokes' law is invalid because of the high Reynolds number. Our strong two-way coupling achieves up to approximately 10% errors and is several orders of magnitude more accurate than one-way and weak two-way coupling.*

η kg/(s·m)	*Re*	$\hat{V}^{\infty}$ m/s	$V^{\infty}_{\text{oneway}}$ m/s	$\varepsilon_{\text{oneway}}(\%)$	V^{∞}_{weak} m/s	$\varepsilon_{\text{weak}}(\%)$	$V^{\infty}_{\text{strong}}$ m/s	$\varepsilon_{\text{strong}}(\%)$
1.0×10^{1}	1.09×10^{1}	1.09×10^{0}	1.65×10^{0}	51.3	0.94×10^{0}	13.6	0.64×10^{0}	41.1
1.0×10^{2}	1.09×10^{-1}	1.09×10^{-1}	1.28×10^{0}	1,073.2	0.52×10^{0}	375.0	0.98×10^{-1}	**10.3**
1.0×10^{3}	1.09×10^{-3}	1.09×10^{-2}	0.57×10^{0}	5,173.4	0.45×10^{0}	4,018.5	1.01×10^{-2}	**6.9**
1.0×10^{4}	1.09×10^{-5}	1.09×10^{-3}	0.94×10^{0}	86,403.3	0.44×10^{0}	40,085.9	1.11×10^{-3}	**1.5**
1.0×10^{5}	1.09×10^{-7}	1.09×10^{-4}	0.67×10^{0}	616,315.8	0.43×10^{0}	396,816.0	1.12×10^{-4}	**2.3**

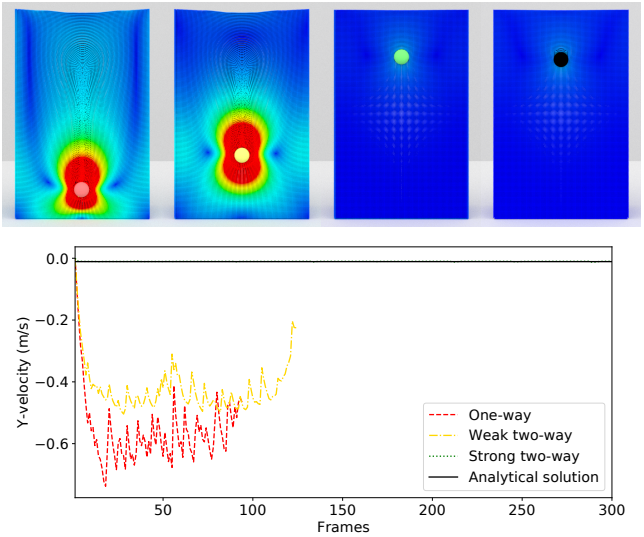

Figure 7: *A solid ball falling inside of fluids with viscosity value $\eta = 1.0\times10^{3}$ kg/(s·m). (Top) From left to right, one-way coupling, weak two-way coupling, and strong two-way coupling. Fluids simulated with one-way and weak two-way coupling cannot sufficiently support the solid ball due to the incorrect viscosity forces while our strong two-way coupling method successfully supports the solid ball. (Bottom) A profile for y-velocity of the solid balls with the analytical solution. The resulting solid velocities with one-way and weak two-way coupling significantly deviate from the analytical solution, whereas the solid velocities given with our strong two-way coupling are in good agreement with the analytical solution.*

the solid ball is treated as prescribed (or kinematic) object in the viscosity solve, giving rise to incorrect fluid and solid dynamics even though viscosity force is applied in the case of weak two-way coupling. On the other hand, the strong two-way coupling method appropriately handles the interplay with viscosity forces between the fluids and the solids in the viscosity solve, leading to the terminal solid velocities close to the analytical solution. Although iterative refinements are possible to improve the accuracy with the weak coupling as implied in [ANZS18], in this scene, the computation time for viscosity solve with one-way, weak two-way, and strong two-way coupling is almost the same and occupies approximately 25–40% of the total simulation time. Thus, we believe that the iterative refinement with weak two-way coupling will become more costly than our strong two-way coupling.

Table 1 summarizes the simulation conditions and results. The velocities of the solid ball simulated with the one-way and weak two-way coupling methods significantly deviate from the analytical solutions whereas our method generates the solid velocities very close to the analytical solutions (relative errors are up to around 10%) except for the case of $\eta = 1.0\times10^{1}$ kg/(s·m), where the Stokes' law is not valid due to the high Reynolds numbers.

We also compared our method with one-way and weak two-way coupling in a more complex scenario, where multiple solid bunnies are dropped onto fluid volumes with spatially varying viscosity values from $\eta = 1.0\times10^{1}$ to 1.0×10^{8} kg/(s·m), as shown in Figure 5. One-way and weak two-way coupling methods do not generate plausible motions nor sufficiently reflect the different viscosity values to the dynamics, whereas our method produces natural behaviors of solid objects as expected with different viscosity values.

4.3. Position Correction

To demonstrate the effectiveness of our position-correction method, we experimented with a scene, where a bulk of viscous fluids is successively compressed by prescribed, solid circular plates with multiple holes, as shown in Figure 8. In this scene, we compared our method with previous approaches using no position correction and position correction based on distance constraints [AT11]. The previous approach without any position corrections easily loses the fluid volumes. While the distance-based position correction better preserves the fluid volumes, still some volumes are lost because this approach is not designed to preserve particle density (and volumes). By contrast, our method directly enforces the uniform particle distributions leading to particle densities closer to the rest density (see particles color-coded based on their densities in Figure 8) and preserving the fluid volumes. This enables fluid volumes to be sufficiently pushed by the solid plates and come out from the holes, reaching the top of the plates.

4.4. Complex Examples

Figure 9 demonstrates three gears two-way coupled with viscous fluids. In this scene, only one rotational DOF for each gear is effective in the viscosity solve, and two rotational and three translational DOFs are eliminated from the system. We note that the two-way

© 2019 The Author(s)
Computer Graphics Forum © 2019 The Eurographics Association and John Wiley & Sons Ltd.

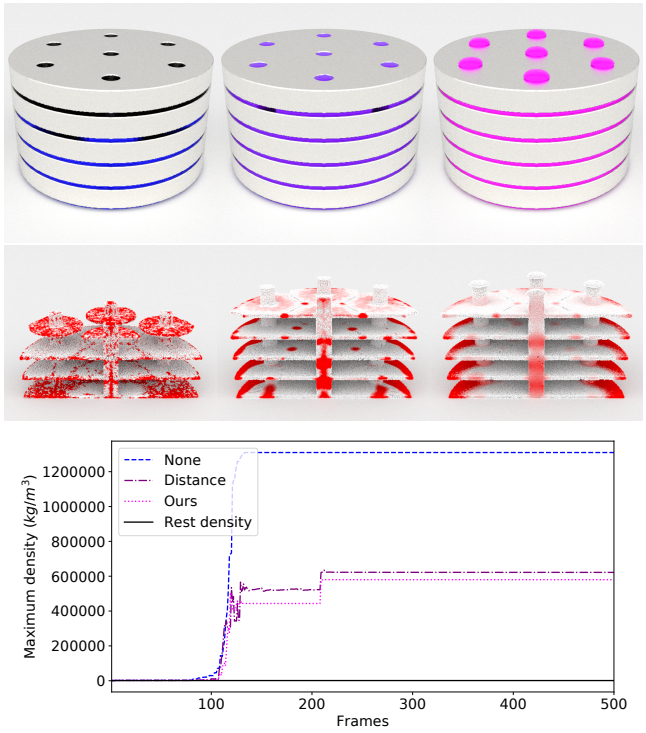

Figure 8: *(Top) A viscous fluid volume successively compressed by prescribed circular plates with several holes. From left to right, no position correction, distance-based position correction, and our method for surface rendering and particle view with color coding (white: low density, red: high density). Because of the density constraint, our method can better preserve the volume of the viscous fluids reaching the top of the plates while other approaches fail to reach the top due to the volume loss. (Bottom) Profile of the maximum particle density, which indicates the inverse of local volumes. Compared to other approaches, our method preserves the density closer to the original one.*

Figure 9: *Three gears interacting with viscous fluids with* $\eta = 1.0 \times 10^1, 1.0 \times 10^2$ *and* 1.0×10^3 $\mathrm{kg}/(\mathrm{s} \cdot \mathrm{m})$ *from left to right. Different viscosity values induce distinct fluid behaviors and solid rotations.*

coupling with viscosity forces accounts for the dragging effects, which can accelerate and decelerate the angular velocities of the gears.

Figure 10 demonstrates complex two-way interactions between multiple solid bunnies and viscous fluids in a rotating drum. Because of the two-way fluid-solid coupling followed by the collision handling between solid objects, interactions between the solid bunnies and the drum in viscous fluids are naturally simulated.

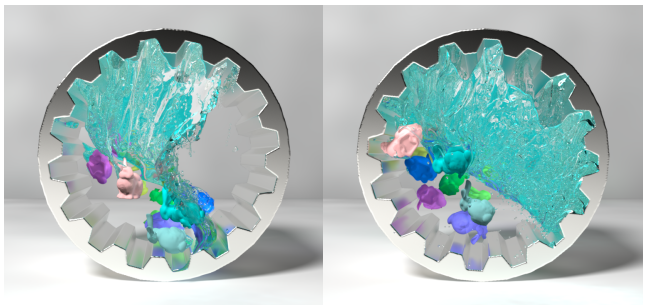

Figure 10: *Multiple solid bunnies interacting with viscous fluids in a rotating drum. Simultaneous one-way (between the bunnies and rotating drum) and two-way (between the bunnies) solid collisions can be addressed by combining our fluid solver with a rigid body solver. Front and back sides are clipped for visualization.*

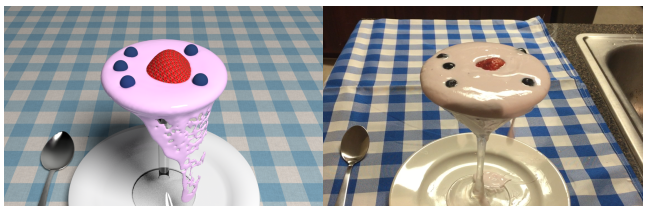

Figure 11: *(Left) Yogurt smoothie overflowing from a cocktail glass because of the dropped strawberry. (Right) Real yogurt smoothie.*

Figure 11 demonstrates the yogurt smoothie interacting with dropped fruits. The yogurt smoothie is pushed by the dropped strawberry and thus overflows from the cocktail glass, as observed in the real phenomena.

4.5. Discussions, Limitations, and Future Work

Volume fractions. In the viscosity solve, we account for the sub-grid geometry with volume fractions based on the variational approach [LBB17]. In the pressure solve, it is known that using the cut-cell method for the fluid-solid interface [NMG09] and ghost fluid method for the liquid-air interface [GFCK02] generally gives more accurate results. However, it is not straightforward to employ these approaches in the viscosity solve, e.g., because the cut-cell methods cannot consistently define the area fractions for velocity components due to changing flux directions with the diagonal and off-diagonal components of the viscous stress. We tested the cut-cell method with a fixed flux direction respecting the diagonal viscous stress components. Although we achieved better accuracy suppressing non-physical oscillations of the solid ball velocities in the scenario shown in Figure 4, we found that neglecting the flux directions of the off-diagonal components leads to popping visual artifacts of particles. Thus, it would be necessary to investigate how to consistently account for the sub-grid geometries to achieve higher accuracy without the artifacts.

Boundary condition. When we consider viscosity formulations with solid objects, it is common to use the no-slip boundary condi-

© 2019 The Author(s)
Computer Graphics Forum © 2019 The Eurographics Association and John Wiley & Sons Ltd.

tion because boundary layers, where viscous forces become dominant, are formed at the proximity of solids in reality. Although this approach works well for fluids with relatively high viscosity values, when fluids are less viscous, the effect of the no-slip boundary condition is magnified up to the scale of simulation cells (which are generally much larger than the thickness of the actual boundary layers) exhibiting excessively viscous behaviors on the boundaries. Using higher resolutions to resolve these issues drastically increases the simulation cost and thus is impractical. One approach to simulating less viscous fluids with solid boundaries is to use fluid velocities instead of solid velocities at the boundaries. In this case, however, the stability of the viscosity solve is not guaranteed, and we encountered the stability issues in our early experiments. Although the use of the free-slip condition or Navier-slip boundary condition for friction is suggested in [Bri15], formulations and implementation become more complex. It would be worthwhile to explore efficient approaches to enforcing these boundary conditions for fluid simulation with a wide range of viscosity values.

Density constraint. The density constraint can resolve the compression of fluids as shown in Figure 8. However, since the density constraint does not attract particles each other, when particles are separating from the others, fluid volumes would suffer from bumps and holes at the limit of the particle resolution. Although attraction forces can be used, we found that the attraction forces cause particle clustering, which is known as the tensile instability in SPH. To address this issue, techniques, such as particle split and merge operations [NGL10], particle sampling [YSB*15], a narrow band approach using the level-set [SWT*18] might be helpful.

Unified solve. While we preferred to decouple pressure and viscosity solves for efficiency, there are certain scenarios, where pressure-viscosity coupled solvers are preferable due to, e.g., capability of coiling, better energy preservation, and more surface details [LBB17]. In addition, the second pressure solve in the decoupled approach would affect the results of the viscosity solve, leading to artificial melting artifacts, e.g., the right most bunny gradually sinking in fluids regardless of the very high viscosity value ($=1.0\times10^8$ kg/(s·m)). Similarly, since our method separately addresses fluid-solid and solid-solid interactions, intensive solid-solid collisions would cause various negative effects, e.g., oscillations of velocity fields and the loss of fluid volumes, both of which can be observed in Figure 5. For future work, we plan to develop a solver that can simultaneously handle pressure and viscosity solves and fluid-solid and solid-solid interactions for robust, accurate, and consistent simulations.

5. Conclusions

We proposed an augmented viscous fluid solver to simulate a wider range of viscous fluid scenarios. Our method offered three key contributions. 1) To avoid the dangling artifacts, we presented a geometrically consistent volume estimation method. 2) We also proposed a new two-way coupling technique that can handle interactions between fluids and solid objects with *viscosity* forces. Our two-way coupling formulation can be seamlessly integrated into the implicit viscosity solve and produces a sparse SPD system monolithically unifying the dynamics of viscous fluids and solid objects. 3) We presented a position-correction method that enforces the uniform distributions of particles to address the volume loss issues, and accelerated the convergence of position corrections with the scaling scheme based on the distance to solid objects. We verified the accuracy of our method by comparing the results with the analytical solutions and demonstrated the effectiveness of our solver in various challenging scenarios.

Acknowledgements

This work is supported in part by National Science Foundation and Elizabeth Stevinson Iribe Chair Professorship. We would like to thank anonymous reviewers for their valuable suggestions and comments.

References

[Aan18] AANJANEYA M.: An efficient solver for two-way coupling rigid bodies with incompressible flow. *Computer Graphics Forum 37*, 8 (July 2018). 3

[AIA*12] AKINCI N., IHMSEN M., AKINCI G., SOLENTHALER B., TESCHNER M.: Versatile rigid-fluid coupling for incompressible SPH. *ACM Transactions on Graphics 31*, 4 (2012), 62:1–62:8. 3

[ANZS18] AKBAY M., NOBLES N., ZORDAN V., SHINAR T.: An extended partitioned method for conservative solid-fluid coupling. *ACM Trans. Graph.* (2018). 3, 7

[AT11] ANDO R., TSURUNO R.: A particle-based method for preserving fluid sheets. In *Proceedings of the 2011 ACM SIGGRAPH/Eurographics Symposium on Computer Animation* (2011), pp. 7–16. 5, 6, 7

[ATW15] ANDO R., THUEREY N., WOJTAN C.: A stream function solver for liquid simulations. *ACM Trans. Graph. 34*, 4 (2015), 53:1–53:9. 3

[Bat08] BATTY C.: Variationalviscosity3D https://github.com/christopherbatty/variationalviscosity3d. 4

[BAV*10] BERGOU M., AUDOLY B., VOUGA E., WARDETZKY M., GRINSPUN E.: Discrete viscous threads. *ACM Transactions on Graphics 29*, 4 (2010), 116:1–116:10. 1, 2

[BB08] BATTY C., BRIDSON R.: Accurate viscous free surfaces for buckling, coiling, and rotating liquids. In *Proceedings of the 2008 ACM SIGGRAPH/Eurographics Symposium on Computer Animation* (2008), pp. 219–228. 1, 2, 3, 6

[BBB07] BATTY C., BERTAILS F., BRIDSON R.: A fast variational framework for accurate solid-fluid coupling. *ACM Trans. Graph. 26*, 3 (July 2007). 1, 2, 3, 5, 6

[BGFAO17] BARREIRO H., GARCÍA-FERNÁNDEZ I., ALDUÁN I., OTADUY M. A.: Conformation constraints for efficient viscoelastic fluid simulation. *ACM Trans. Graph. 36*, 6 (2017), 221:1–221:11. 2

[BH11] BATTY C., HOUSTON B.: A simple finite volume method for adaptive viscous liquids. In *Proceedings of the 2011 ACM SIGGRAPH/Eurographics Symposium on Computer Animation* (2011), pp. 111–118. 2

[BK16] BENDER J., KOSCHIER D.: Divergence-free sph for incompressible and viscous fluids. *IEEE Transactions on Visualization and Computer Graphics PP*, 99 (2016), 1–1. 2

[Bri15] BRIDSON R.: *Fluid Simulation for Computer Graphics*. A K Peters/CRC Press, 2015. 2, 4, 5, 6, 9

[BUAG12] BATTY C., URIBE A., AUDOLY B., GRINSPUN E.: Discrete viscous sheets. *ACM Transactions on Graphics 31*, 4 (2012), 113:1–113:7. 1, 2

[CGFO06] CHENTANEZ N., GOKTEKIN T. G., FELDMAN B. E., O'BRIEN J. F.: Simultaneous coupling of fluids and deformable bodies. In *Proceedings of the 2006 ACM SIGGRAPH/Eurographics Symposium on Computer Animation* (2006), pp. 83–89. 1, 2

[CMT04] CARLSON M., MUCHA P. J., TURK G.: Rigid fluid: Animating the interplay between rigid bodies and fluid. *ACM Trans. Graph. 23*, 3 (2004), 377–384. 1, 2

© 2019 The Author(s)
Computer Graphics Forum © 2019 The Eurographics Association and John Wiley & Sons Ltd.

[CMVHT02] CARLSON M., MUCHA P. J., VAN HORN III R. B., TURK G.: Melting and flowing. In *Proceedings of the 2002 ACM SIGGRAPH/Eurographics Symposium on Computer Animation* (2002), pp. 167–174. 1, 2

[DBD16] DAVIET G., BERTAILS-DESCOUBES F.: A semi-implicit material point method for the continuum simulation of granular materials. *ACM Trans. Graph. 35*, 4 (2016), 102:1–102:13. 2, 3

[GBO04] GOKTEKIN T. G., BARGTEIL A. W., O'BRIEN J. F.: A method for animating viscoelastic fluids. *ACM Trans. Graph. 23*, 3 (2004), 463–468. 2, 3

[GFCK02] GIBOU F., FEDKIW R. P., CHENG L.-T., KANG M.: A second-order-accurate symmetric discretization of the poisson equation on irregular domains. *Journal of Computational Physics 176*, 1 (2002), 205 – 227. 8

[GPH*18] GAO M., PRADHANA A., HAN X., GUO Q., KOT G., SIFAKIS E., JIANG C.: Animating fluid sediment mixture in particle-laden flows. *ACM Trans. Graph.* (2018). 2

[GSLF05] GUENDELMAN E., SELLE A., LOSASSO F., FEDKIW R.: Coupling water and smoke to thin deformable and rigid shells. *ACM Trans. Graph. 24*, 3 (2005), 973–981. 2

[HFG*18] HU Y., FANG Y., GE Z., QU Z., ZHU Y., PRADHANA A., JIANG C.: A moving least squares material point method with displacement discontinuity and two-way rigid body coupling. *ACM Trans. Graph.* (2018). 2, 3

[JGT17] JIANG C., GAST T., TERAN J.: Anisotropic elastoplasticity for cloth, knit and hair frictional contact. *ACM Trans. Graph. 36*, 4 (2017), 152:1–152:14. 2, 3

[JSS*15] JIANG C., SCHROEDER C., SELLE A., TERAN J., STOMAKHIN A.: The affine particle-in-cell method. *ACM Trans. Graph. 34*, 4 (July 2015), 51:1–51:10. 3

[KFCO06] KLINGNER B. M., FELDMAN B. E., CHENTANEZ N., O'BRIEN J. F.: Fluid animation with dynamic meshes. *ACM Trans. Graph. 25*, 3 (2006). 1, 2

[KGP*16] KLÁR G., GAST T., PRADHANA A., FU C., SCHROEDER C., JIANG C., TERAN J.: Drucker-prager elastoplasticity for sand animation. *ACM Trans. Graph. 35*, 4 (2016), 103:1–103:12. 2, 3

[KLL*07] KIM B., LIU Y., LLAMAS I., JIAO X., ROSSIGNAC J.: Simulation of bubbles in foam with the volume control method. *ACM Trans. Graph. 26*, 3 (2007). 5

[LBB17] LARIONOV E., BATTY C., BRIDSON R.: Variational stokes: A unified pressure-viscosity solver for accurate viscous liquids. *ACM Trans. Graph. 36*, 4 (July 2017), 101:1–101:11. 1, 2, 3, 4, 6, 8, 9

[LJF16] LU W., JIN N., FEDKIW R.: Two-way coupling of fluids to reduced deformable bodies. In *Proceedings of the ACM SIGGRAPH/Eurographics Symposium on Computer Animation* (2016), pp. 67–76. 1, 3

[MG07] MIN C., GIBOU F.: Geometric integration over irregular domains with application to level-set methods. *Journal of Computational Physics 226*, 2 (2007), 1432 – 1443. 4

[MMCK14] MACKLIN M., MÜLLER M., CHENTANEZ N., KIM T.-Y.: Unified particle physics for real-time applications. *ACM Transactions on Graphics 33*, 4 (2014), 153:1–153:12. 3, 5, 6

[NGL10] NARAIN R., GOLAS A., LIN M. C.: Free-flowing granular materials with two-way solid coupling. *ACM Transactions on Graphics 29*, 6 (2010), 173:1–173:10. 2, 4, 5, 9

[NMG09] NG Y. T., MIN C., GIBOU F.: An efficient fluid-solid coupling algorithm for single-phase flows. *Journal of Computational Physics 228*, 23 (2009), 8807 – 8829. 6, 8

[PICT15] PEER A., IHMSEN M., CORNELIS J., TESCHNER M.: An implicit viscosity formulation for sph fluids. *ACM Trans. Graph. 34*, 4 (2015), 114:1–114:10. 1, 2

[PT17] PEER A., TESCHNER M.: Prescribed velocity gradients for highly viscous sph fluids with vorticity diffusion. *IEEE Transactions on Visualization and Computer Graphics 23*, 12 (2017), 2656–2662. 2

[REN*04] RASMUSSEN N., ENRIGHT D., NGUYEN D., MARINO S., SUMNER N., GEIGER W., HOON S., FEDKIW R.: Directable photorealistic liquids. In *Proceedings of the 2004 ACM SIGGRAPH/Eurographics Symposium on Computer Animation* (2004), pp. 193–202. 1, 2

[RMEF09] ROBINSON-MOSHER A., ENGLISH R. E., FEDKIW R.: Accurate tangential velocities for solid fluid coupling. In *Proceedings of the 2009 ACM SIGGRAPH/Eurographics Symposium on Computer Animation* (2009), SCA '09, pp. 227–236. 3

[RMSF11] ROBINSON-MOSHER A., SCHROEDER C., FEDKIW R.: A symmetric positive definite formulation for monolithic fluid structure interaction. *J. Comput. Phys. 230*, 4 (Feb. 2011), 1547–1566. 2, 3

[RMSG*08] ROBINSON-MOSHER A., SHINAR T., GRETARSSON J., SU J., FEDKIW R.: Two-way coupling of fluids to rigid and deformable solids and shells. *ACM Trans. Graph. 27*, 3 (2008), 46:1–46:9. 1, 2, 5

[SSC*13] STOMAKHIN A., SCHROEDER C., CHAI L., TERAN J., SELLE A.: A material point method for snow simulation. *ACM Trans. Graph. 32*, 4 (2013), 102:1–102:10. 2

[SSJ*14] STOMAKHIN A., SCHROEDER C., JIANG C., CHAI L., TERAN J., SELLE A.: Augmented MPM for phase-change and varied materials. *ACM Transactions on Graphics 33*, 4 (2014), 138:1–138:11. 2

[SSP07] SOLENTHALER B., SCHLÄFLI J., PAJAROLA R.: A unified particle model for fluid-solid interactions. *Computer Animation and Virtual Worlds 18*, 1 (2007), 69–82. 3

[Sta99] STAM J.: Stable fluids. In *Proceedings of the 26th Annual Conference on Computer Graphics and Interactive Techniques* (1999), pp. 121–128. 2

[SWT*18] SATO T., WOJTAN C., THUEREY N., IGARASHI T., ANDO R.: Extended Narrow Band FLIP for Liquid Simulations. *Computer Graphics Forum* (2018). 9

[TBV12] TONGE R., BENEVOLENSKI F., VOROSHILOV A.: Mass splitting for jitter-free parallel rigid body simulation. *ACM Trans. Graph. 31*, 4 (2012), 105:1–105:8. 6

[TDF*15] TAKAHASHI T., DOBASHI Y., FUJISHIRO I., NISHITA T., LIN M. C.: Implicit formulation for SPH-based viscous fluids. *Computer Graphics Forum 34*, 2 (2015), 493–502. 1, 2

[TGK*17] TAMPUBOLON A. P., GAST T., KLÁR G., FU C., TERAN J., JIANG C., MUSETH K.: Multi-species simulation of porous sand and water mixtures. *ACM Trans. Graph. 36*, 4 (2017), 105:1–105:11. 2

[TLK16] TENG Y., LEVIN D. I. W., KIM T.: Eulerian solid-fluid coupling. *ACM Trans. Graph. 35*, 6 (2016), 200:1–200:8. 1, 3

[UBH14] UM K., BAEK S., HAN J.: Advanced hybrid particle-grid method with sub-grid particle correction. *Comput. Graph. Forum 33*, 7 (2014), 209–218. 5

[VHLL14] VINES M., HOUSTON B., LANG J., LEE W.-S.: Vortical inviscid flows with two-way solid-fluid coupling. *IEEE Transactions on Visualization and Computer Graphics 20*, 2 (Feb. 2014), 303–315. 3

[Wan13] WANG S.: 3D volume calculation for the marching cubes algorithm in cartesian coordinates. *Arxiv* (2013). 4

[WKBB18] WEILER M., KOSCHIER D., BRAND M., BENDER J.: A physically consistent implicit viscosity solver for sph fluids. *Computer Graphics Forum (Eurographics) 37*, 2 (2018). 2

[YSB*15] YUE Y., SMITH B., BATTY C., ZHENG C., GRINSPUN E.: Continuum foam: A material point method for shear-dependent flows. *ACM Trans. Graph. 34*, 5 (2015), 160:1–160:20. 2, 9

[ZB17] ZARIFI O., BATTY C.: A positive-definite cut-cell method for strong two-way coupling between fluids and deformable bodies. pp. 7:1–7:11. 1, 3

[ZLQF15] ZHU B., LEE M., QUIGLEY E., FEDKIW R.: Codimensional non-newtonian fluids. *ACM Trans. Graph. 34*, 4 (2015), 115:1–115:9. 1, 2

© 2019 The Author(s)
Computer Graphics Forum © 2019 The Eurographics Association and John Wiley & Sons Ltd.